Journal of
Materials Chemistry B

PAPER

View Article Online
View Journal

Cite this: DOI: 10.1039/c9tb00375d

Multifunctional Gd-based mesoporous silica nanotheranostic for anticancer drug delivery†

Fabio Carniato, ‡[a] Diego Alberti, ‡[b] Angelica Lapadula,[bc] Jonathan Martinelli,[a] Ciro Isidoro, [c] Simonetta Geninatti Crich [b] and Lorenzo Tei *[a]

Received 24th February 2019,
Accepted 5th April 2019

DOI: 10.1039/c9tb00375d

rsc.li/materials-b

A nanosized drug delivery system based on mesoporous silica nanoparticles functionalized with highly stable GdDOTAGA complexes, rhodamine dyes and PEG_{3000} molecules was synthesized. The external side of the PEG was also functionalized with azadibenzocyclooctyne moieties in order to exploit the bioorthogonal Cu(I)-free click chemistry targeting approach after metabolic labeling of cell-surface glycans with azido-mannose molecules. The particles' pores were then impregnated with the chemotherapeutic drug mitoxantrone to add a therapeutic function to the nanosystem. The bioorthogonal targeting of the nanotheranostic probe on mannose-treated breast cancer MCF7 and TS/A cells showed a minimal difference between cells metabolically labeled or not. However, MRI experiments on labeled MCF7 cells showed a significant 200% contrast enhancement with respect to untreated cells, thus confirming the high contrast efficiency even when the cells were incubated with nanoparticles for a few minutes. Moreover, administration of the nanoprobe to MCF7 cultures resulted in a higher cytotoxicity in comparison to the free drug at a similar concentration, confirming the successful delivery of the drug.

1. Introduction

Theranostics is a newly emerging concept aimed at developing imaging procedures able to provide a non-invasive *in vivo* visualization of therapeutic treatments. A theranostic system enables obtaining more accurate pharmacokinetics and drug delivery data, such as overall biodistribution, organ delivery success and targeting efficiency. This novel biomedical approach requires the use of chemical species containing in the same structure both diagnostic and therapeutic agents.[1–3] A typical theranostic protocol requires an imaging reporter able to visualize a specific biomarker that characterizes the pathology of interest and/or is involved in the mechanism of action of the therapeutic treatment. Thus, the efficacy of the therapy can be determined by looking at the changes in the imaging response of the biomarker. Among the available imaging modalities, magnetic resonance imaging (MRI) shows peculiar advantages over the other available techniques such as impressive spatial resolution of soft tissues, very low invasiveness, optimal temporal resolution and outstanding versatility. On the other hand, the greatest disadvantage of MRI is its relatively poor sensitivity, which requires the use of contrast agents at high concentration in order to visualize the desired biomarker.[4] This drawback can be overcome by using nanocarriers (micelles, liposomes, inorganic/organic nanoparticles) that, typically, are the same cargos employed to improve the therapeutic index of many drugs. Great efforts have been made in this direction, as testified by the reviews and articles published in the last few decades within this field.[5–7] Various nano-devices have been proposed for the construction of novel theranostic agents including multifunctional nanoparticles (NPs), polymeric micelles, and liposomes, often enriched with iron oxide NPs or paramagnetic metal ions.[8–11] Among them, mesoporous silica nanoparticles (MSNs) have also been considered for the generation of a new family of nanoformulations.[12–15]

Many researchers have focused their studies on the development of MSNs optimized for controlled drug delivery. In 2001, Vallet-Regí *et al.* for the first time investigated the release of anti-inflammatory drugs entrapped in MCM-41 pores.[16] More recently, MSNs functionalized with different drugs and decorated with different biocompatible (*i.e.* phospholipid layers)[17] and target molecules (folic acid, peptides, and specific ligands)[18] have been proposed as efficient drug delivery systems.

In parallel, MSNs have also been exploited for the development of T_1 MR-enhancing hybrid materials based on gadolinium(III) complexes anchored onto the MSN surface.[19] Initial studies reported on the anchoring of the chelates on MSNs, with different

[a] Department of Science and Technological Innovation, Università del Piemonte Orientale, Viale T. Michel 11, 15121 Alessandria, Italy. E-mail: lorenzo.tei@uniupo.it
[b] Department of Molecular Biotechnology and Health Science, University of Turin, Via Nizza 52, 10126 Torino, Italy
[c] Department of Health Sciences, Università del Piemonte Orientale, Via Solaroli 17, 28100, Novara, Italy

† Electronic supplementary information (ESI) available: Supplementary figures. See DOI: 10.1039/c9tb00375d

‡ These authors contributed equally to this work.

shapes and sizes, aimed to increase the ^{1}H relaxivity of the system for cell tracking and angiographic MRI applications.[20] More recently, studies in our laboratories on the anchoring of different Gd(III) complexes on the internal or external surfaces of MSNs and on the modification of the surface functionalities have led us to optimize the nanoprobe, reaching very high relaxivities.[19,21–23] The final outcome is that Gd(III) chelates have to be anchored onto the external surface of the MSNs because water diffusion inside the pores is limited and this prevents the transfer of the paramagnetic effect to the bulk water. A synthetic procedure for the preparation of efficient GdDOTA-like chelates anchored onto the MSN external surface was developed resulting in a very high relaxivity of the system.[21]

Nevertheless, it must be noted that the combination in the same nanoparticles of both drug molecules and MRI contrast agents has marginally been explored. The few examples reported in the literature described the preparation of hybrid organic–inorganic MSNs containing drug molecules (*e.g.* doxorubicin) and functionalized with T_2-contrast agents, such as Fe_2O_3,[24] or the use of the hollow space between a stable iron nanocore and a mesoporous silica shell to load anticancer drugs and GdDTPA molecules.[25] Interestingly, Kempen *et al.* developed theranostic MSNs offering both ultrasound and MRI signals to monitor the delivery of insulin growth factor to mesenchymal stem cells.[26]

However, optimization of all functionalities present in the same MSN platform, in terms of enhanced imaging contrast, controlled drug release and selective uptake, is a challenge for the research in the theranostic field. In particular, all these functions in the final theranostic probe should work without losing efficiency and, therefore, an accurate design of the synthetic procedure is required. Some *in vitro* examples have been reported showing the influence of the mutual interactions between the drug, the Gd(III) chelates and the silica surface on the effectiveness of the final theranostic system.[27] In another system, the selective surface functionalization of MCM-48 nanoparticles by GdDTPA-monoamide and polyethylene glycol (PEG) molecules allowed optimization of the drug (daunorubicin) loading and release performances, avoiding pore obstruction.[28]

Herein we independently functionalized the three well-defined domains of MSNs by anchoring MRI contrast agents, a fluorescent dye, PEG molecules and targeting groups onto the MSN surface, and confining drug molecules inside the pores. Based on our previous studies on Gd-functionalized MSNs,[21,22] we chose GdDOTAGA complexes (DOTAGA = (*R*)-2-(4,7,10-triscarboxymethyl-1,4,7,10-tetraazacyclododec-1-yl)pentanedioic acid) as MRI agents anchored onto the silica surface. In fact, GdDOTAGA is a thermodynamically stable, kinetically inert, mononegative GdDOTA-like system with one inner-sphere water molecule with an optimal water exchange rate ($\tau_M = 1/k_{ex} = ca.$ 100 ns)[29] that allows obtaining high relaxivities when attached to the silica surface. Then, PEG molecules were grafted at the outer surface of MSNs to improve their colloidal stability under physiological conditions, as well as bio- and hemocompatibility.[30] Moreover, PEGylation usually increases the blood circulation half-life time reducing the detection of the NPs by the reticuloendothelial system and allows higher accumulation of NPs at tumor sites. Another functionalization was carried out on the MSN surface to enable the targeting of membrane monosaccharide sialic acid (SA) residues, which are relevant biomarkers of the metastatic activity of tumors.[31] To reach this goal we used the bioorthogonal copper-free click chemistry approach proposed by Bertozzi *et al.*[32,33] based on metabolic labeling of cell-surface glycans using an azide-containing analog of acetylated mannose, *N*-azidoacetyl-D-mannosamine (Ac_4ManNAz). This approach has been widely applied also *in vivo* for cancer cell labeling and targeted delivery of NPs.[34–40] Thus, the functionalization of the MSN surface with a strained cyclooctyne derivative, located at the end terminus of a long PEG chain, allows exploiting the Cu-free click chemistry approach *in vitro* and *in vivo* by local inoculation of the azido-modified sugar. The surface of MSNs was also labeled with a fluorescent dye (rhodamine), in order to enable the visualization of NPs in the cells. Finally, the chemotherapeutic drug mitoxantrone (MTX), an anthraquinone derivative that has been extensively investigated for the treatment of breast and prostate cancer,[41] was confined into the MSN pores. This drug has been chosen as Oupický *et al.* have recently demonstrated the efficient loading and release of this water-soluble weak electrolyte drug into amino- and thiol-surface modified MSNs.[42] In the present work, the properties of each functionality (the contrast efficiency, the modulation of the drug release and the particle uptake in malignant tissues) have been evaluated in detail.

2. Results and discussion

2.1. Synthesis and physico-chemical characterization

A schematic illustration of the multifunctional nanotheranostic probe is shown in Fig. 1. The first synthetic step was the preparation of the organo-modified mesoporous silica containing aminopropyl groups exposed on the surface. The synthesis was carried out following the traditional sol–gel procedure assisted by the presence

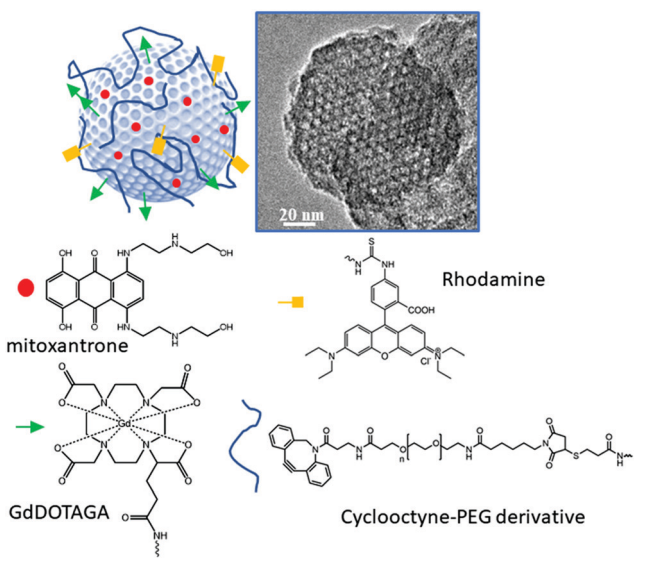

Fig. 1 A schematic illustration and HRTEM micrograph of the theranostic probe (MTX-Gd-CyPEG-MSN).

of Pluronic F127 and the cationic surfactant hexadecyltrimethylammonium chloride (CTAC). The amino groups were introduced *via* a one-pot approach during the gel preparation, using aminopropyltriethoxysilane as the precursor. As indicated by high-resolution TEM micrographs, such a synthetic procedure allowed us to obtain particles with size below 100 nm, in agreement with MSNs prepared by a similar approach (Fig. 1).[22] Moreover, the TEM images indicate the presence of a regular porosity along the entire spheroidal nanoparticle. Further details on the physico-chemical properties of these porous nanoparticles have been described previously.[21,22]

The cyclooctyne-PEG (Cy-PEG, Scheme S3, ESI†) derivative was synthesized in two steps by reacting azadibenzo-cyclooctynamine with Mal-PEG3000-NHS followed by Michael addition of mercapto-propionic acid to the terminal maleimide. The surface functionalization of the organo-modified MSN with GdDOTAGA and Cy-PEG_{3000} molecules was carried out by reacting the *in situ* activated carboxylic acid groups to the NH_2 groups present on the silica surface (Gd-CyPEG-MSN). A reference sample prepared in a similar way but containing non-functionalized PEG_{3000} was also synthesized (hereafter named Gd-PEG-MSN). The surface of the two MSN samples was finally labeled with rhodamine B isothiocyanate, which formed a thiourea bond with the amino functionalities of the organo-modified silica. The average amount of Gd^{3+} chelates attached to the surface, estimated by ICP-AES elemental analysis, was 22 (22 650 Gd^{3+} ions per particle) and 44 μmol g^{-1} (45 300 Gd^{3+} ions per particle) for Gd-CyPEG-MSN and Gd-PEG-MSN samples, respectively (Table 1). The loading of the dye present in both NPs was estimated by UV/Vis spectroscopy. Spectroscopic data indicate that 0.12 and 0.32 μmol g^{-1} of fluorophore are attached to Gd-CyPEG-MSN and Gd-PEG-MSN, respectively (Fig. S1, ESI† and Table 1). The cyclooctyne-PEG moiety in the Gd-CyPEG-MSN sample was also quantified by UV–visible titration with a cyanine dye containing an azide group (Cy5.5-azide, Scheme S1, ESI†) that can react by a Cu(I)-free click chemistry reaction with the cyclooctyne group. Using this method we determined the excess amount of Cy5.5-azide that remained in the liquid phase after reaction in water with the CyPEG derivative attached to the silica surface (Fig. S2, ESI†), by analyzing the visible absorption band of cyanine at 675 nm. The amount of azadibenzo-cyclooctyne molecules was estimated to be 50 μmol g^{-1} (Table 1).

The behavior of the functionalized samples in aqueous solutions appeared markedly different with respect to the unmodified MSNs. For the latter, we observed a heterogeneous particle size distribution (determined by DLS analysis) centered at 180 nm. In contrast, for both Gd-CyPEG-MSN and Gd-PEG-MSN samples the hydrodynamic radius distribution appeared narrow with a maximum value of 110 nm (Fig. 2). In addition, we improved the suspension stability over time, which remained substantially constant for *ca.* 10 days (Fig. 2B). These results can be attributed to the presence of PEG molecules on the particle surface that improves the solubility and prevents aggregation. Moreover, the functionalized silica particles showed a slightly positive charge density (zeta-potential) of +2.0 ± 0.5 mV, exposed on the surface, due to the presence of residual non-functionalized NH_3^+ groups.

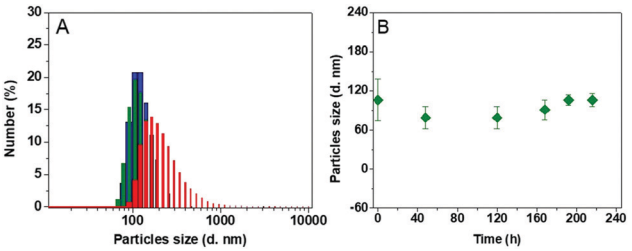

Fig. 2 (A) DLS analysis at 298 K of MSNs (red), Gd-PEG-MSNs (blue) and Gd-CyPEG-MSNs (green) in aqueous solution; and (B) stability of the aqueous suspension of Gd-CyPEG-MSNs over time.

The electronic properties of both dye-functionalized NPs were investigated by UV/Vis and photoluminescence (PL) spectroscopy (Fig. S3, ESI†). The UV/Vis spectrum of rhodamine in water shows absorption maxima attributed to the π → π* transitions (λ = 525 and 557 nm); the same bands are observed after conjugation of the dye to MSNs. Moreover, the PL spectra of both rhodamine and dye-functionalized MSNs, recorded in aqueous solution, display an emission band with a maximum at 580 nm (Fig. S3, ESI†).

2.2. ^{1}H NMR relaxometric characterization

The ^{1}H NMR relaxometric properties of Gd-CyPEG-MSN and Gd-PEG-MSN were investigated in aqueous solution at neutral pH and 298 K to evaluate the efficacy of the theranostic probe as an imaging reporter. The efficacy of an MRI contrast agent can be determined by the longitudinal relaxivity parameter (r_1) that corresponds to the variation in the relaxation rates of water protons normalized to 1 mM concentration of the paramagnetic probe. The r_1 values at 0.47 T (20 MHz) for Gd-CyPEG-MSN and Gd-PEG-MSN are 49.2 ($r_1 \approx 1.1 \times 10^6$ per particle) and 45.7 mM^{-1} s^{-1} ($r_1 \approx 2.1 \times 10^6$ per particle), respectively. These values are *ca.* 10 times higher than that of the discrete GdDOTAGA complex, in agreement with the results reported previously on MSN samples selectively functionalized on the external surface with the same Gd chelates.[21] These values are sensibly higher (more than 50%) than those measured for other theranostic Gd-based systems in which the Gd-complex anchored onto the silica surface was a GdDOTA-monoamide[27] or GdDTPA-monoamide.[28] This result confirms the importance of anchoring onto the silica surface an anionic GdDOTA-like complex, such as GdDOTAGA,

Table 1 Quantification of the organic functionalities confined in different samples

	[Gd^{3+}]/μmol g^{-1}	[Rhodam]/μmol g^{-1}	[CyOct]/μmol g^{-1}	[MTX]/μmol g^{-1}
Gd-PEG-MSN	44	0.32	—	—
Gd-CyPEG-MSN	22	0.12	50	—
MTX-Gd-CyPEG-MSN	22	0.12	50	1.6

which presents a faster water exchange rate of the coordinated water molecule ($k_{ex} \sim 7 \times 10^6$ s^{-1}) with respect to GdDOTA- or GdDTPA-monoamides. The other important factor to consider is the stability of the macrocyclic Gd-complexes anchored onto the NP surface: GdDOTAGA chelates ensure excellent *in vitro* and *in vivo* stability and an improved safety profile with respect to transmetallation by endogenous metal ions or transchelation by endogenous anions.

In particular, it is well-established that high relaxivity values in the 20–60 MHz (0.5–1.5 T) magnetic field strength range are related to a restriction of the molecular tumbling motion of the complex when conjugated to the particle surface.[5] Based on the high r_1 values observed for both samples, we hypothesize that most of the GdDOTAGA complexes are accessible to water molecules, which are mainly distributed on the external surface. To get more insight into the molecular parameters affecting r_1, the proton relaxation rate was measured as a function of the magnetic field strength, from 1.0 to 60 MHz at 298 K, obtaining a so-called Nuclear Magnetic Relaxation Dispersion (NMRD) profile. Both Gd-CyPEG-MSN and Gd-PEG-MSN show similar profiles characterized by the presence of a broad peak with maximum at 20 MHz, typical of paramagnetic macromolecular systems with hindered rotation dynamics (Fig. 3).

The physico-chemical parameters of the paramagnetic MSNs can be determined by analyzing the NMRD profiles according to well-established theoretical models based on the Solomon–Bloembergen–Morgan equations.[4] For paramagnetic chelates attached to NPs, the rotational mobility is better analyzed by following the Lipari–Szabo model free approach. Such a model distinguishes the rapid local rotation of the complex (τ_{RL}) from the global motion of the entire NP (τ_{RG}). The coupling of local and global motions is defined by the parameter S^2 that varies between 1 (global and local motions coincide) and 0 (local and global motions are completely independent).[43,44] The best-fit was achieved by fixing the number of water molecules directly coordinated to the metal ion to 1 ($q = 1$), the distance between the metal and protons of the inner sphere water molecule (r_{GdH}) to 3.0 Å and τ_{RG} to 0.1 ms in agreement with paramagnetic MSNs previously reported (Table 2).[11–14] The electronic parameters (Δ^2 and τ_V) were introduced in the fitting as empirical parameters because they do not have a real physical meaning for nanosized systems.

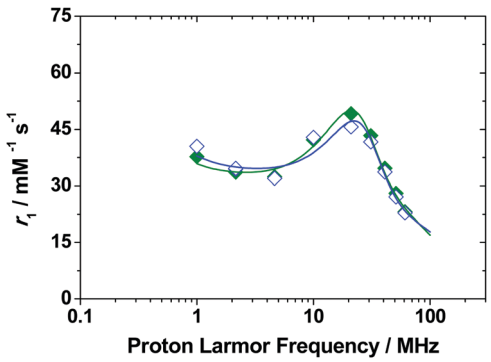

Fig. 3 ^{1}H NMRD profiles at 298 K of Gd-PEG-MSN (blue) and Gd-CyPEG-MSN (green) samples. The best-fit curves were calculated using the parameters in Table 2.

Table 2 Selected best-fit parameters obtained from the analysis of ^{1}H NMRD profiles of Gd-PEG-MSN and Gd-CyPEG-MSN at 298 K[a]

Parameters	Gd-PEG-MSN	Gd-CyPEG-MSN
$^{20}r_1$ [mM^{-1} s^{-1}]	45.7	49.2
τ_{RG} [ms]	0.1	0.1
τ_{RL} [ns]	0.99 ± 0.51	1.52 ± 0.47
τ_M [ns]	124 ± 9	162 ± 5
S^2	0.37 ± 0.13	0.45 ± 0.08

[a] The following parameters were fixed to common values during the fitting procedure: $r_{Gd\text{-}H}$ = 3.0 Å, a = 4.0 Å, $D = 2.3 \times 10^{-5}$ cm^2 s^{-1}.

The parameters that significantly influence the r_1 values at high magnetic fields are τ_{RL}, S^2 and the inner sphere water residence lifetime (τ_M). The local mobility of the complex in both samples is restricted owing to the conjugation to the silica surface. The local rotational correlation time is *ca.* 1 ns for both materials, more than two orders of magnitude higher with respect to the re-orientational correlation time of the free complex. The value of S^2 around 0.4 confirms the restricted mobility of the complexes around the linker to the NP.[5] The mean residence lifetime of the coordinated water molecule was 124 and 162 ns for Gd-PEG-MSN and Gd-CyPEG-MSN, respectively, similar to the values obtained for MSNs functionalized on the external surface with GdDOTAGA chelates[21] and only slightly higher that that measured for mononuclear GdDOTAGA.[29]

2.3. Drug loading and release

The theranostic agent was finally prepared by impregnating Gd-CyPEG-MSNs with the chemotherapeutic drug mitoxantrone (MTX-Gd-CyPEG-MSN). Mitoxantrone is a DNA intercalating drug that inhibits DNA duplication and transcription, and is used for the treatment of breast cancer, lymphoma and leukaemia. This step was carried out in water at room temperature for 24 h. The amount of drug in the MSNs was 1.6 μmol g^{-1} (*ca.* 0.7 mg g^{-1}), as determined by fluorescence spectroscopy (Fig. S4, ESI†). This amount is lower than that observed in non-functionalized MSNs,[42] clearly due to the presence of multiple entities on the surface of NPs (Gd-complexes, rhodamine and PEG molecules) that hinders access to the pores. The release of MTX from NPs was assessed at 37 °C under dialysis. The MTX showed an initial rapid release of about 60% of the total drug within the first 3 hours, followed by a slower and continuous release (Fig. 4), in agreement with the data already reported in the literature for non-functionalized MSNs.[42] The high initial burst release can be attributed to the dissolution of MTX physically adhered to the surface or located in the first layers of the solid NPs.

2.4. Evaluation of the efficiency of bio-orthogonal labeling with ADIBO-FITC

Two mammary cancer cell lines, one human (MCF7) and one murine (TS/A), were used for the preliminary assessment of the correct exposure of Ac_4ManNAz on the cell surface. To this end, the cells were incubated in the presence of an Ac_4ManNAz solution (50 μM in 0.25 v/v% ethanol in cell medium) for

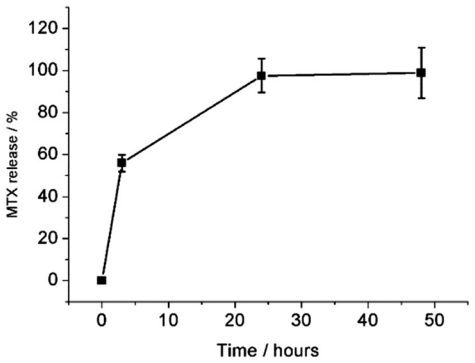

Fig. 4 *In vitro* MTX release from MTX-Gd-CyPEG-MSNs evaluated at different times (3, 24, and 48 h) under dialysis in water at 37 °C. The bars show the mean SE of % MTX release obtained from three independent experiments.

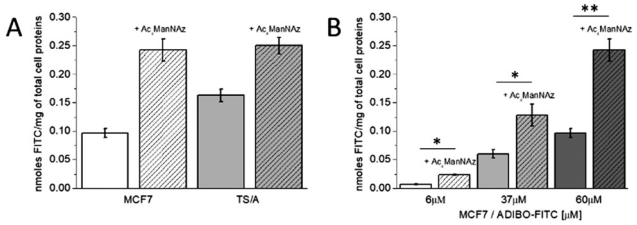

Fig. 5 Spectrofluorimetric analysis of (A) MCF7 and TS/A cells labeled with 60 μM ADIBO-FITC pre-incubated in the presence or in the absence of Ac_4ManNAz and (B) MCF7 cells labeled with 6–60 μM ADIBO-FITC pre-incubated in the presence or in the absence of Ac_4ManNAz. Fluorescence values measured for cell lysates (upon treatment with 0.1% Triton) were normalized to the total cell protein content determined by Bradford assay. Error bars correspond to ±SE. *$p < 0.05$. **$p < 0.01$. Student *t*-test.

72 hours at 37 °C (5% CO_2). Azide-modified sugars were incorporated through existing biosynthetic pathways both onto the cell surface and in internal glycans. After incorporation, the azide groups were available for reaction with the dye ADIBO-FITC containing a cyclooctyne moiety (Scheme S2, ESI†).[45] The reaction was carried out by incubating both cell lines for 60 min at 37 °C in the presence of 60 μM ADIBO-FITC (0.2 v/v% ethanol in cell medium). Then cell labeling was assessed by measuring the fluorescence intensity of cell lysates in 0.1% Triton in phosphate buffer saline (PBS) (Fig. 5A), after extensive washing in PBS.

The amount of FITC that remains bound to the cells was normalized to the total cell protein content. Fig. 5A shows that the ADIBO-FITC cell binding is significantly higher in cells pre-incubated with the Ac_4ManNAz sugar and that labeling efficiency is higher in the case of human MCF7. The next experiments were carried out only on this cell line. Fig. 5B shows the direct correlation between ADIBO-FITC concentration used during the incubation and labeling efficiency. In the range of concentrations considered, the saturation of Ac_4ManNAz residues was not yet reached.

2.5. Labeling of MCF7 with Gd-CyPEG-MSNs

To the best of our knowledge, the bio-orthogonal targeting strategy has not yet been used with functionalized MSNs. In fact, Chiu *et al.* reported the preparation and characterization of cyclooctyne-modified MSNs in which the Cu(I)-free click chemistry approach was used for conjugation of a dye molecule to the MSN surface, and not for cellular targeting.[46]

Using the same experimental protocol discussed above, 0.5 million MCF7 were incubated in the presence of Gd-CyPEG-MSNs directly re-suspended in the cell medium. In fact, the presence of 10% serum concentration reduces the nanoparticle aggregation and the average Gd-CyPEG-MSN diameter remains at *ca.* 120 nm for about 20 min. For this reason, a very short incubation time (10 min at room temperature), sufficient for the bioorthogonal reaction,[47] was used to avoid Gd-CyPEG-MSN aggregation over time. In fact, the azadibenzocyclooctyne moieties on the nanoprobe's surface were chosen as they are reported to undergo a fast click reaction with azides[47] also under *in vivo* conditions. Fig. 6 shows that after 10 min incubation at room temperature, similar amounts of NPs (measured by rhodamine fluorescence and Gd measurements by ICP-MS) are taken-up by the MCF7 cells, either pre-incubated or not with Ac_4ManNAz.

As possible explanations, the cyclooctyne group was not sufficiently available for the reaction with the azide group on the cell membrane (likely because of its folding towards the MSN surface) or simply the background signal generated by the extremely fast non-specific MSNs binding covered the specific one, even when using PEG-coated MSNs. Indeed, the few examples of successful bioorthogonal two step labeling strategies based on nanosized probes were performed by using NPs with a lower unspecific affinity for the cell surface (glycol chitosan NPs or liposomes).[34,35,39]

Another possibility is related to the hydrophobic nature of the dibenzocyclooctyne that could make it less available for targeting. Therefore, the use of bicyclononynes could provide a good balance in terms of reactivity and hydrophilicity, thus improving the targeting efficiency.[48,49]

The unspecific affinity of Gd-CyPEG-MSNs for the cell surface was confirmed by MRI analysis of T_1-weighted images. As shown in Fig. 7, although a strong signal enhancement (*ca.* 200%) was observed with respect to untreated cells, the pre-incubation with Ac_4ManNAz does not affect the signal intensity of cell pellets and their corresponding R_1 measured at 7 T. This result confirms that the high relaxivity showed by Gd-complexes conjugated to the MSN external surface allowed the observation of a remarkable contrast even when the cells were incubated with the MSNs for a few minutes.

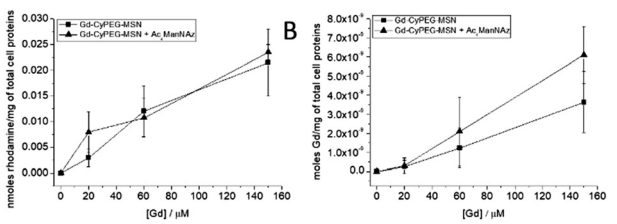

Fig. 6 Spectrofluorimetric (A) and ICP-MS (B) analysis of MCF7 cells labeled with Gd-CyPEG-MSNs (20–150 μM Gd) pre-incubated in the presence or in the absence of Ac_4ManNAz. The amount of rhodamine and Gd measured for cell lysates was normalized to the total cell protein content determined by Bradford assay. Error bars correspond to ±SE.

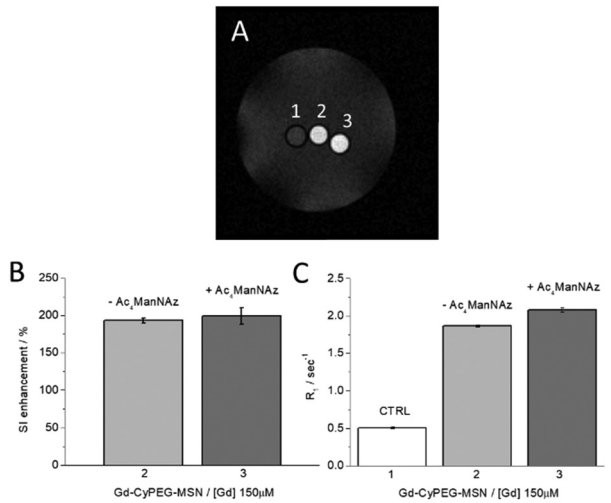

Fig. 7 T_1-weighted MRI image (A), % SI enhancements (B) and longitudinal relaxation rates R_1 (C); analyses of an agar phantom containing glass capillaries with MCF7 cell pellets: untreated cells (1) and cells previously labeled with Gd-Cy-PEG-MSNs pre-incubated either in the absence (2) or the presence (3) of Ac_4ManNAz. Error bars correspond to ±SE.

2.6. Cytotoxicity test of MSNs embedded with MTX (MTX-Gd-CyPEG-MSNs)

MCF7 cell vitality was determined by the MTT assay. The cells were incubated for 10 min in the presence of MTX-Gd-CyPEG-MSNs and MTX alone, at a 1–12.5 μM concentration range. After washing, the cells were left 24 h in a fresh medium before MTT. MTX toxicity was evaluated for both cells pre-incubated and not pre-incubated with Ac_4ManNAz for 72 h. Fig. 8A shows that the toxicity of MTX loaded in MSNs is significantly higher than that observed with MTX incubated alone at the same concentration. In fact, 10 min is a short incubation time and the amount of MTX internalized, when incubated alone, is not sufficient to induce a significant cell toxicity and the vitality remains >60% also at high MTX concentrations (12.5 μM) (Fig. 8A). Instead, delivery of MSNs significantly increased the rate of MTX internalization due to their affinity for the cell surface. As a result, cell vitality decreased to less than 40% at high MTX concentrations. Cell vitality was not significantly different in cultures pre-incubated or not with Ac_4ManNAz, confirming that MSNs do not increase the amount of MTX delivered through the binding to the azide group on the sugar moiety. Furthermore, the amount of MTX found associated with cells was determined after 10 min incubation of MTX-Gd-CyPEG-MSNs. This was extrapolated by ICP-MS Gd concentration measurements using the ratio Gd/MTX = 12 found in naked NPs. The same amount of pure MTX was added to the culture medium to test its cytotoxicity in MCF7 cells. Data in Fig. 8B show that MTX released by MSNs elicits a cytotoxic effect higher than that of free MTX administered at the same ratio, supporting the conclusion that theranostics is more efficient in delivering the drug to the target cells.

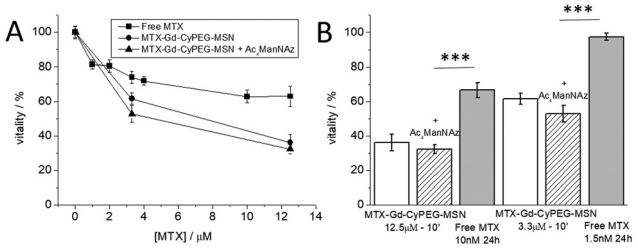

Fig. 8 Cytotoxicity assay (MTT) of Gd-CyPEG-MSNs embedded with MTX (Gd-MTX-CyPEG-MSNs). Error bars correspond to ±SE. ***$p < 0.001$, Student t-test.

3. Experimental

3.1. Materials

2-(*R*)-2-(4,7,10-Triscarboxy-methyl-1,4,7,10-tetraazacyclododec-1-yl) pentanedioic acid = DOTAGA was purchased from Chematech (France). Mitoxantrone was purchased from 3V Chimica S.r.l. (Italy). Mal-PEG3000-NHS and azadibenzocyclooctinamine were purchased from Iris Biotech GmbH (Germany). Cy5.5-azide (Scheme S1, ESI†) was purchased from Lumiprobe GmbH. ADIBO-FITC (Scheme S2, ESI†) and Ac_4ManNAz were synthesized as reported previously.[45] All other materials and solvents were purchased from Sigma-Aldrich and used without further purification.

3.2. Synthesis

GdDOTAGA. The Gd(III) complex was prepared by adding an equimolar amount of $GdCl_3$ solution to the ligand solution in water, maintaining the pH at 6.5 with diluted sodium hydroxide. The solution was stirred overnight at 298 K and the pH was corrected to 9 in order to promote the precipitation of unreacted Gd^{3+} as $Gd(OH)_3$. The suspension was then centrifuged at 4000 rpm for 5 min and the solution was filtered using 0.2 μm filters. Finally, the solvent was removed under reduced pressure leading to the formation of a white solid. ESI-MS: *m*/*z* calcd for the complex ($C_{19}H_{27}GdN_4O_{10}$): 628.7; found: 628.5 [$M - H^+$]. The peak attributed to the Gd(III)-complex showed the correct isotopic distribution.

Cy-PEG-Mal (Scheme S3a, ESI†). Mal-PEG3000-NHS (50 mg) was dissolved in DCM (7 mL). Azadibenzocyclooctinamine (6 mg) was added to the solution, and the mixture was stirred at room temperature overnight. The resulting solution was poured into an excess of Et_2O (30×) and the obtained suspension was centrifuged (4000 rpm, 30 min, 10 °C). The supernatant was discarded and the remaining solid was washed/centrifuged with Et_2O (3 × 10 mL) and dried under vacuum. The product (white solid, 41 mg) was used without further purification (Fig. S5a, ESI†). ^{1}H NMR ($CDCl_3$, 500 MHz, 25 °C): 7.38 (m, 8H), 6.69 (s, 2H), 6.54 (bs, 1H), 6.09 (bs, 1H), 5.15 (d, 1H), 3.8–3.4 (m, *x*H), 3.30 (m, 2H), 2.47 (m, 1H), 2.32 (m, 2H), 2.16 (m, 2H), 1.98 (m, 1H), 1.63 (m, 4H), and 1.31 (m, 2H). ^{13}C NMR ($CDCl_3$, 125 MHz, 25 °C): 172.8 (CO), 172.0 (CO), 171.1 (CO), 170.9 (CO), 151.1 (C^{Ar}), 148.1 (C^{Ar}), 134.1 (CH^{Mal}), 132–114 (CH^{Ar} + C^{Ar}), 109.3 ($\underline{C}\equiv C$), 107.8 ($C\equiv\underline{C}$), 71–65 (OCH_2), 55.5 (CH_2^{CyOct}), 39.2 (NCH_2), 37.1 ($NHCH_2$), 37.7 ($NHCH_2$), 36.4 ($COCH_2$), 35.2 ($COCH_2$), 34.8 ($COCH_2$), 28.4 (CH_2), 26.5 (CH_2), and 25.2 (CH_2).

Cy-PEG-COOH (Scheme S3b, ESI†). Mal-PEG3000-CyOct (40 mg) was dissolved in DCM (5 mL) and mercaptopropionic acid (4 μL) was added. The solution was stirred at room temperature overnight and poured into an excess of Et_2O (30×). The resulting precipitate was centrifuged (4000 rpm, 30 min, 10 °C) and washed/centrifuged with Et_2O (3 × 10 mL). After drying under vacuum, a white solid (38 mg) was obtained, which was used without further purification (Fig. S5b, ESI†). ^{1}H NMR ($CDCl_3$, 500 MHz, 25 °C): 7.3–7.0 (m, 8H, Ar), 6.66 (bs, 1H, m), 6.62 (bs, 1H, g), 4.62 (d, 1H), 3.76 (CHS), 3.7–3.4 (m, $[OCH_2CH_2O]_n$), 2.92 (m, 2H, CH_2CHS), 2.69 (SCH_2), 2.52 (CH_2COOH), 2.44 (m, 1H), 2.24 (m, 2H), 2.18 (m, 2H), 2.15 (m, 1H), 1.85 (m, 2H), 1.60 (m, 2H), and 1.28 (m, 2H). ^{13}C NMR ($CDCl_3$, 125 MHz, 25 °C): 177.3 (CO), 175.4 (CO), 174.3 (CO), 172.6 (CO), 142.0 (C^{Ar}), 132–128 (CH^{Ar} + C^{Ar}), C≡C resonances are too broad to be observed, 71–65 (OCH_2), 54.2 (CH_2^{CyOct}), 40.3 (CHS), 39.9 ($NHCH_2$), 39.4 (NCH_2), 37.5 ($NHCH_2$), 36.7 (CO$\underline{C}H_2$), 35.4 (CO$\underline{C}H_2$), 34.9 ($\underline{C}H_2$COOH), 34.4 ($\underline{C}H_2$CHS), 33.9 (CO$\underline{C}H_2$), 26.9 (CH_2), 26.3 (CH_2), 26.1 (CH_2), and 25.8 (CHS).

Synthesis of organo-modified MSN nanoparticles. The MSN nanoparticles were synthesized following the procedure described in the literature.[13] In detail, tetraethoxysilane (TEOS) (3.15 g, 15 mmol) and aminopropyl triethoxysilane (APTS) (0.37 g, 1.7 mmol) were dissolved in 30 g of a diluted hydrochloric acid solution (0.3 mol L^{-1}) at room temperature along with 2.6 g of cetyltrimethylammonium chloride and 2.0 g of Pluronic F127. After stirring for 3 h at room temperature, 3.0 g of ammonia solution (14.7 mol L^{-1}) were added to the suspension. The final gel was stirred at RT for 24 h, transferred to an autoclave at 60 °C for another 24 h and centrifuged at 4000 rpm for 5 min. The gel was transferred to a dialysis membrane (Sigma Aldrich, molecular weight cut-off 14 000), and dialyzed in 500 mL acid solution containing 250 mL of water, 250 mL of ethanol and 5 mL of acetic acid for 24 h in order to remove surfactant molecules. The procedure was repeated three times and finally dialysis in 1 L of deionized water for 8 h was also carried out.

Preparation of Gd-CyPEG-MSN and Gd-PEG-MSN. A DMF suspension (40 mL) containing 200 mg of MSN nanoparticles was stirred for a few minutes at room temperature. In parallel, 90.7 mg of GdDOTAGA, 106.2 mg of HBTU and 37 mg of HOBT were dissolved in 5 mL of DMF. After complete dissolution of the samples, 33 mg of Cy-PEG-COOH and 100 μL of DIPEA were added. The final solution was added to the MSN suspension and stirred for 18 h at RT. The suspension was then centrifuged at 7000 rpm at 10 °C in order to isolate the nanoparticles. In the last step, the particles were suspended in 40 mL of water containing 300 μL of the rhodamine solution previously prepared by dissolving 1.24 mg of the dye in 10 mL of water. The suspension was stirred at RT for 8 h and centrifuged at 7000 rpm for 10 min at 10 °C. After removal of the solvent, the particles were resuspended in water. Gd-PEG-MSN was prepared by a similar procedure.

The Gd loading per particle was determined by assuming a spherical shape for the particles and a density of 0.8 g cm^{-3} for the Gd-CyPEG-MSN and Gd-PEG-MSN samples.[22] The concentration of the cyclooctyne group on the silica surface was quantified by UV–visible titration with a cyanine probe containing an azide group (Cy5.5-azide, Scheme S1, ESI†). The silica nanoparticles in aqueous solution were treated with the dye for 15 min and then centrifuged. The excess amount of Cy5.5-azide that remained in the liquid phase after the reaction was analysed by UV–visible spectroscopy by evaluating the absorption band of cyanine at 675 nm (Fig. S2, ESI†).

Impregnation of mitoxantrone in Gd-CyPEG-MSN and drug release assay. 10 mL of an aqueous suspension containing 50 mg of CyPEG-MSN were stirred for 10 min at room temperature. 14 mg of mitoxantrone were dissolved in the suspension. The impregnation reaction was maintained by stirring for 24 h at RT. Finally, the suspension was centrifuged and a blue powder was isolated.

After MTX-Gd-CyPEG-MSN resuspension in water at a concentration of 0.2 mM Gd (as by ICP-AES), aliquots of the sample (200 μL) were centrifuged for 10 min at 7500 rpm and the silica were resuspended in 2 mL of DMSO in order to determine the MTX concentration. The concentration of drug was quantified by measuring the fluorescence intensity according to a MTX calibration curve (Ex 620 nm Em 692 nm in the range of 0.1–2 μM) using a spectrofluorimeter HORIBA Jobin Yvon Fluoromax-4, Edison, NY, USA.

To perform the drug release assay, following the procedure described above, 1.5 mL of MTX-Cy-PEG-MSNs at a 0.2 mM Gd concentration in water were dialyzed at 37 °C (MWCO 14 kDa) in 40 mL water for 48 h. At 0, 3, 24 and 48 h time intervals, 200 μL of the dialyzed MTX-Gd-CyPEG-MSNs were taken and centrifuged for 10 min at 7500 rpm. Then, after removing the supernatant buffer, the MTX-Gd-CyPEG-MSNs were resuspended in 2 mL of DMSO. The 40 mL dialysis solution was renewed at each drawing. The percentage of MTX released was calculated using the equation:

$$\%\ \text{release} = \frac{\text{MTX}(t_0) - \text{MTX}(t_i)}{\text{MTX}(t_0)} \times 100$$

for which MTX (t_i) is the amount of MTX loaded in MTX-Gd-CyPEG-MSNs measured by spectrofluorimetry at various time intervals (t = 0, 3, 24, and 48 h), and MTX (t_0) is the amount of MTX loaded in MTX-Gd-CyPEG-MSNs at the starting point (t = 0) of the drug release test.

3.3. Characterization techniques

The elemental analyses were carried out using a Spectro Genesis inductively-coupled plasma atomic emission spectrometer equipped with a cross-flow nebulizer (ICP-AES). Prior to the analyses, the samples were mineralized by treatment with a mixture of HNO_3 (5 mL) and HF (5 mL) at 100 °C for 8 h.

The chromatographic analyses were carried out using a Waters high-performance liquid chromatography–mass spectrometry system equipped with an electrospray ion source (HPLC-MS ESI+/−), a Waters 1525 Binary HPLC pump, a Waters 2489 UV-Vis detector and a Waters SQD 3100 mass detector. The mass spectra, obtained through the MS-ESI+/− technique, were recorded using the Waters SQD 3100 mass detector.

High-resolution transmission electron microscopy (HRTEM) images were collected using a JEOL 3010 High Resolution

Transmission Electron Microscope operating at 300 kV. The specimens were prepared by depositing the samples on carbon-coated grids.

The UV–vis spectra were recorded at RT in the range 200–900 nm with a resolution of 1 nm, using a double-beam PerkinElmer Lambda 900 spectrophotometer.

Dynamic light scattering experiments (DLS) were carried out at 25 °C by using a Malvern Zetasizer NanoZS operating in the particle size range from 0.6 nm to 6 mm and equipped with a He–Ne laser with λ = 633 nm.

The water proton longitudinal relaxation rates as a function of the magnetic field strength were measured in non-deuterated aqueous solutions using a Fast Field-Cycling Stelar SmarTracer relaxometer (Stelar s.r.l., Mede (PV), Italy) over a continuum of magnetic field strengths from 0.00024 to 0.25 T (corresponding to 0.01–10 MHz proton Larmor frequencies). The relaxometer operates under computer control with an absolute uncertainty in $1/T_1$ of ±1%. Additional longitudinal relaxation data in the range 20–70 MHz were obtained using a Stelar Relaxometer connected to a Bruker WP80 NMR electromagnet adapted to variable-field measurements. The ^{1}H T_1 relaxation times were acquired by the standard inversion recovery method with a typical 90° pulse width of 3.5 μs, 16 experiments of 4 scans. The temperature was controlled using a Stelar VTC-91 airflow heater equipped with a calibrated copper-constantan thermocouple (uncertainty of ±0.1 °C). The concentration of Gd^{3+} ions for each analysed suspension was measured by ^{1}H NMR (500 MHz) experiments using the Evans method.[50]

3.4. Biological analyses

Human MCF7 breast cancer cell line was purchased from American Type Culture Collection (ATCC, USA) and murine TS/A breast cancer cell line was kindly provided by Prof. F. Cavallo's group, University of Turin. The MCF7 cells were cultured in EMEM (Lonza) supplemented with 10% (v/v) fetal bovine serum (FBS), 2 mM glutamine, 100 U mL^{-1} penicillin, 100 U mL^{-1} streptomycin, 1 mM sodium pyruvate, non-essential amino acids, and 10 μg mL^{-1} insulin (Sigma). The TS/A cells were cultured in RPMI (Lonza) supplemented with 10% (v/v) FBS, 4 mM glutamine, 100 U mL^{-1} penicillin and 100 U mL^{-1} streptomycin.

For ADIBO-FITC labelling experiments, 2.5 × 10^5 MCF7 and TS/A cells were seeded in 6 cm diameter Petri dishes. After 24 h, they were incubated in the absence or in the presence of 50 μM Ac_4ManNAz (0.25 v/v% ethanol in medium, Lonza) for 72 h at 37 °C and 5% CO_2. After the incubation, the cells were washed three times with phosphate buffer saline (PBS) and incubated for another 1 h at 37 °C and 5% CO_2 in the presence of different concentrations (6–60 μM) of ADIBO-FITC (0.2 v/v% ethanol in medium). Then, the cells were washed three times with PBS, detached using 1 mM EDTA (ethylenediaminetetraacetic acid), resuspended in 250 μL of PBS, sonicated in ice at 30% power for 30 s and assayed for their protein content by the Bradford method. Then, the samples were diluted 1 : 10 in 0.1% Triton in PBS and analyzed for their FITC fluorescence according to a FITC calibration curve (Ex 492 nm Em 517 nm in the range 0.5–30 nM). The obtained nanomoles of FITC calculated for each cell sample were normalized to milligrams of total cell proteins measured by Bradford assay.

For Gd-CyPEG-MSN uptake experiments, 9 × 10^4 MCF7 cells were seeded in 6 well plates. After 24 h, they were incubated in the absence or in the presence of 50 μM Ac_4ManNAz for 72 h at 37 °C and 5% CO_2. After the incubation, they were washed three times with PBS and incubated for another 10 minutes at room temperature (RT) in the presence of different concentrations of Gd-CyPEG-MSNs (20–150 μM Gd). Then, the cells were washed three times with PBS, detached using 1 mM EDTA, re-suspended in 200 μL of PBS, sonicated in ice at 30% power for 30 s and assayed for their protein content by the Bradford method. Then, the samples were diluted in Triton (0.1% final concentration) and analysed for their fluorescence by a Promega Glomax-Multi + Detection System according to a rhodamine B calibration curve (Ex 525 nm Em 580–640 nm in the range 5–200 nM). The obtained nanomoles of rhodamine B calculated for each cell sample were normalized to milligrams of total cell proteins measured by Bradford assay. Finally, after fluorescence analysis, the Gd amount in each cell sample was evaluated by ICP-MS. Digestion was performed by heating under microwave (Milestone Ethos Up Microwave Digestion System) 0.2 mL of cell suspensions for 20′ at 160 °C, after the addition of 0.2 mL of concentrated HNO_3 (70%). After mineralization, 3 mL of ultrapure water were added to the remaining sample volumes for inductively coupled plasma mass spectrometry (ICP-MS; element-2; Thermo-Finnigan, Rodano (MI), Italy).

MRI studies. According to the above mentioned protocol for Gd-CyPEG-MSN uptake experiments, about 5 × 10^5 MCF7 cells treated or not treated with Ac_4ManNAz, incubated with Gd-CyPEG-MSNs for 10 minutes at RT (150 μM Gd), were transferred to glass capillaries placed in an agar phantom. The MR images were obtained using a standard T_1-weighted multi slice spin echo sequence (TR (repetition time)/TE (echo time)/NEX number of excitations) = 250/3.7/6, FOV (field of view) = 1.2 cm) connected to a Bruker Avance300 spectrometer (7 T) provided with a Micro 2.5 microimaging probe (Bruker BioSpin, Ettlingen, Germany). $1/T_1$ relaxation rates were determined using a standard Saturation Recovery Spin Echo.

The mean signal intensity (SI) values were calculated in the regions of interest (ROI) drawn on T_1 weighted images of the cell pellet samples. The mean SI enhancement (%) of cells treated with Gd-CyPEG-MSN was calculated according to the following equation: SI% enhancement = ((mean SI (treated cells) − mean SI (untreated cells)/mean SI (untreated cells)) × 100.

MTT assay. The MTT assay is based on the reduction of tetrazolium salts to formazan using mitochondrial succinate dehydrogenase, which is quantified by a spectrophotometer. MCF7 cells were seeded at a density of 5 × 10^3 cells per well in a 96-well microtiter plate and treated in the presence or in the absence of 50 μM Ac_4ManNAz for 72 h, and after washing with PBS the cells were incubated with MTX-Gd-CyPEG-MSNs or with free MTX for 10 minutes at RT (3.3–12.5 μM MTX). After this time, the incubation medium was removed and renewed with a 100 μL of fresh medium for another 24 h. Then, this medium was removed and each well was incubated with thiazolyl

blue tetrazolium bromide dissolved in the medium at a concentration of 0.45 mg mL^{-1} for 4 h at 37 °C and 5% CO_2. Then, after medium elimination, 150 μL of DMSO were added into each well to solubilize the formazan salt crystals produced by the metabolism of live cells and the microplate was incubated at room temperature for 30 min. Finally, absorbance was measured at 570 nm using an iMark microplate reader (Biorad). Cell vitality was reported as the percentage of dead cells observed in the treated samples relative to that observed in the non-treated control cells. Moreover, to assess the cytotoxic effect of free MTX incubated for a longer time, the same amount of MTX found associated with cells after 10′ incubation with MTX-Gd-CyPEG-MSNs was incubated alone for 24 h in the cell medium and then MTT was performed. The amount of MTX internalized by MTX-Gd-CyPEG-MSNs after 10 min incubation was extrapolated by the amount of cell internalized Gd measured by ICP-MS (see above), using the calculated Gd/MTX molar ratio in MSN of 12. In this way, it was estimated that upon incubation of MTX-Gd-CyPEG-MSNs at 3.3 and 12.5 μM MTX concentration (10 min at RT), 1.5×10^{-4} nmoles and 1×10^{-3} nmoles of MTX were taken up by the cells, respectively.

4. Conclusions

This work describes the development and characterization of MRI-based theranostic MSNs as biocompatible nanocarriers that simultaneously display improved physical–chemical properties and multiple functions including: (i) good chemical stability and versatility, (ii) high surface area and tunable pore size, (iii) great potential for anchoring several different chemical entities, (iv) good dispersibility, (v) high loading of MRI contrast agents, (vi) high contrast efficiency (high relaxivity), (vii) good delivery of poorly water-soluble drugs, and (viii) optimized drug biodistribution through targeted delivery of therapeutics.

In detail, the points (i–iii) include properties that are typical of MSNs and that have pushed their development in the biomedical field in recent years. The other properties were implemented by a multifunctional MSN probe that is equipped with: (1) thermodynamically stable and kinetically inert Gd-complexes allowing high relaxivity, (2) PEG molecules that increase the aqueous solubility of the NPs (which might increase the half-time in blood circulation), (3) rhodamine molecules for the spectrofluorimetric analysis of the cellular uptake and localization of MSNs, and (4) a PEGylated cyclooctyne group that permits the targeting of membrane monosaccharide sialic acid (SA) residues *via* the bioorthogonal Cu(I)-free click chemistry approach. The synthetic procedure for the multi-functionalization of the MSN platform was carefully designed in order to obtain the best performance of any single function. As a result, the multifunctional probe Gd-CyPEG-MSN shows a very high relaxivity per Gd ion (49.2 mM^{-1} s^{-1}), which is found to be a relaxivity per particle of more than 1.1×10^6 mM^{-1} s^{-1}.

Despite the efficient metabolic azido labeling of the MCF7 and TS/A cell surface, Gd-CyPEG-MSN bioorthogonal binding was negligible and no significant difference between the MCF7 cells metabolically labeled or not with azido-mannose was observed. However, our results show that the (unspecific) affinity of the nanoprobe for the cell surface is sufficient for the successful delivery of an anticancer drug (such as the MTX used here), eliciting a cytotoxic effect higher than that obtained with the same concentration of free drug. Moreover, the high relaxivity showed by Gd-complexes conjugated to the MSNs enabled us to obtain a significant contrast enhancement even after very short incubation times. Thus, in conclusion, we have developed an efficient theranostic nanosystem in terms of diagnostic capability and drug release efficacy that could be used either to exploit the enhanced permeability retention effect without the use of a targeting moiety or in targeted theranostics by changing or improving the targeting ability.

Conflicts of interest

There are no conflicts to declare.

Acknowledgements

The authors acknowledge Euro-BioImaging (www.eurobioimaging.eu) for providing access to imaging technologies and services *via* the Multi-Modal Molecular Imaging Italian Node (Torino, Italy). FC, JM, CI and LT acknowledge the financial support from Compagnia di San Paolo (CSP-2014 THERASIL Project).

Notes and references

1 T. Lammers, S. Aime, W. E. Hennink, G. Storm and F. Kiessling, *Acc. Chem. Res.*, 2011, **44**, 1029–1038.
2 E. Terreno, F. Uggeri and S. Aime, *J. Controlled Release*, 2012, **161**, 328–337.
3 V. J. Yao, S. D'Angelo, K. S. Butler, C. Theron, T. L. Smith, S. Marchio, J. G. Gelovani, R. L. Sidman, A. S. Dobroff, C. J. Brinker, A. R. M. Bradbury, W. Arap and R. Pasqualini, *J. Controlled Release*, 2016, **240**, 267–286.
4 A. E. Merbach, L. Helm and E. Tòth, *The chemistry of contrast agents in medical magnetic resonance imaging*, John Wiley & Sons, New York, 2nd edn, 2013.
5 M. Botta and L. Tei, *Eur. J. Inorg. Chem.*, 2012, 1945–1960.
6 D. D. Castelli, E. Gianolio, S. G. Crich, E. Terreno and S. Aime, *Coord. Chem. Rev.*, 2008, **252**, 2424–2443.
7 A. J. L. Villaraza, A. Bumb and M. W. Brechbiel, *Chem. Rev.*, 2010, **110**, 2921–2959.
8 J. T. Cole and N. B. Holland, *Drug Delivery Transl. Res.*, 2015, **5**, 295–309.
9 M. S. Muthu, D. T. Leong, L. Mei and S. S. Feng, *Theranostics*, 2014, **4**, 660–677.
10 J. H. Ryu, S. Lee, S. Son, S. H. Kim, J. F. Leary, K. Choi and I. C. Kwon, *J. Controlled Release*, 2014, **190**, 477–484.
11 J. Xie, S. Lee and X. Y. Chen, *Adv. Drug Delivery Rev.*, 2010, **62**, 1064–1079.
12 J. E. Lee, N. Lee, T. Kim, J. Kim and T. Hyeon, *Acc. Chem. Res.*, 2012, **44**, 893–902.

13 J. Liu, T. T. Liu, J. Pan, S. M. Liu and G. Q. Lu, *Annu. Rev. Chem. Biomol. Eng.*, 2018, **9**, 389–411.
14 M. Vallet-Regi, F. Balas and D. Arcos, *Angew. Chem., Int. Ed.*, 2007, **46**, 7548–7558.
15 J. L. Vivero-Escoto, R. C. Huxford-Phillips and W. B. Lin, *Chem. Soc. Rev.*, 2011, **41**, 2673–2685.
16 M. Vallet-Regí, A. Ramila, R. P. del Real and J. Perez-Pariente, *Chem. Mater.*, 2001, **13**, 308–311.
17 Y. Yang, W. X. Song, A. H. Wang, P. L. Zhu, J. B. Fei and J. B. Li, *Phys. Chem. Chem. Phys.*, 2010, **12**, 4418–4422.
18 Z. L. Wang, B. Xu, L. Zhang, J. B. Zhang, T. H. Ma, J. B. Zhang, X. Q. Fu and W. J. Tian, *Nanoscale*, 2013, **5**, 2065–2072.
19 F. Carniato, L. Tei and M. Botta, *Eur. J. Inorg. Chem.*, 2018, 4936–4954.
20 J. K. Hsiao, C. P. Tsai, T. H. Chung, Y. Hung, M. Yao, H. M. Liu, C. Y. Mou, C. S. Yang, Y. C. Chen and D. M. Huang, *Small*, 2008, **4**, 1445–1452.
21 F. Carniato, L. Tei, A. Arrais, L. Marchese and M. Botta, *Chem. – Eur. J.*, 2013, **19**, 1421–1428.
22 F. Carniato, L. Tei, M. Cossi, L. Marchese and M. Botta, *Chem. – Eur. J.*, 2010, **16**, 10727–10734.
23 F. Carniato, L. Tei, W. Dastru, L. Marchese and M. Botta, *Chem. Commun.*, 2009, 1246–1248.
24 J. E. Lee, N. Lee, H. Kim, J. Kim, S. H. Choi, J. H. Kim, T. Kim, I. C. Song, S. P. Park, W. K. Moon and T. Hyeon, *J. Am. Chem. Soc.*, 2010, **132**, 552–557.
25 M. Y. Wu, Q. S. Meng, Y. Chen, P. F. Xu, S. J. Zhang, Y. P. Li, L. X. Zhang, M. Wang, H. L. Yao and J. L. Shi, *Adv. Funct. Mater.*, 2014, **24**, 4273–4283.
26 P. J. Kempen, S. Greasley, K. A. Parker, J. L. Campbell, H. Y. Chang, J. R. Jones, R. Sinclair, S. S. Gambhir and J. V. Jokerst, *Theranostics*, 2015, **5**, 631–642.
27 F. Carniato, M. Munoz-Ubeda, L. Tei and M. Botta, *Dalton Trans.*, 2015, **44**, 17927–17931.
28 M. Bouchoucha, R. C-Gaudreault, M. A. Fortin and F. Kleitz, *Adv. Funct. Mater.*, 2014, **24**, 5911–5923.
29 F. Kielar, L. Tei, E. Terreno and M. Botta, *J. Am. Chem. Soc.*, 2010, **132**, 7836–7837.
30 G. E. Francis, C. Delgado, D. Fisher, F. Malik and A. K. Agrawal, *J. Drug Targeting*, 1996, **3**, 321–340.
31 I. Martinez-Duncker, R. Salinas-Marin and C. Martinez-Duncker, *Int. J. Mol. Imaging*, 2011, **2011**, 283497.
32 P. V. Chang, J. A. Prescher, E. M. Sletten, J. M. Baskin, I. A. Miller, N. J. Agard, A. Lo and C. R. Bertozzi, *Proc. Natl. Acad. Sci. U. S. A.*, 2010, **107**, 1821–1826.
33 E. M. Sletten and C. R. Bertozzi, *Angew. Chem., Int. Ed.*, 2009, **48**, 6974–6998.
34 H. Koo, S. Lee, J. H. Na, S. H. Kim, S. K. Hahn, K. Choi, I. C. Kwon, S. Y. Jeong and K. Kim, *Angew. Chem., Int. Ed.*, 2012, **51**, 11836–11840.
35 S. Lee, H. Koo, J. H. Na, S. J. Han, H. S. Min, S. J. Lee, S. H. Kim, S. H. Yun, S. Y. Jeong, I. C. Kwon, K. Choi and K. Kim, *ACS Nano*, 2014, **8**, 2048–2063.
36 R. Xie, L. Dong, Y. F. Du, Y. T. Zhu, R. Hua, C. Zhang and X. Chen, *Proc. Natl. Acad. Sci. U. S. A.*, 2016, **113**, 5173–5178.
37 R. Xie, S. L. Hong, L. S. Feng, J. Rong and X. Chen, *J. Am. Chem. Soc.*, 2012, **134**, 9914–9917.
38 G. Yi, J. Son, J. Yoo, C. Park and H. Koo, *Biomater. Res.*, 2018, **22**, 13.
39 H. I. Yoon, J. Y. Yhee, J. H. Na, S. Lee, H. Lee, S. W. Kang, H. Chang, J. H. Ryu, S. Lee, I. C. Kwon, Y. W. Cho and K. Kim, *Bioconjugate Chem.*, 2016, **27**, 927–936.
40 H. Y. Yoon, H. Koo, K. Kim and I. C. Kwon, *Biomaterials*, 2017, **132**, 28–36.
41 B. J. Evison, B. E. Sleebs, K. G. Watson, D. R. Phillips and S. M. Cutts, *Med. Res. Rev.*, 2016, **36**, 248–299.
42 A. Wani, E. Muthuswamy, G. H. L. Savithra, G. Z. Mao, S. Brock and D. Oupický, *Pharm. Res.*, 2012, **29**, 2407–2418.
43 G. Lipari and A. Szabo, *J. Am. Chem. Soc.*, 1982, **104**, 4546–4559.
44 G. Lipari and A. Szabo, *J. Am. Chem. Soc.*, 1982, **104**, 4559–4570.
45 D. Alberti, C. Grange, S. Porta, S. Aime, L. Tei and S. G. Crich, *ACS Omega*, 2018, **3**, 8097–8103.
46 H. Y. Chiu, D. Goss, L. Haddick, H. Engelke and T. Bein, *Chem. Mater.*, 2018, **30**, 644–654.
47 J. C. Jewett, E. M. Sletten and C. R. Bertozzi, *J. Am. Chem. Soc.*, 2010, **132**, 3688–3690.
48 J. Dommerholt, S. Schmidt, R. Temming, L. J. A. Hendriks, F. P. J. T. Rutjes, J. C. M. van Hest, D. J. Lefeber, P. Friedl and F. L. van Delft, *Angew. Chem., Int. Ed.*, 2010, **49**, 9422–9425.
49 H. Tian, T. P. Sakmar and T. Huber, *Chem. Commun.*, 2016, **52**, 5451–5454.
50 D. M. Corsi, C. Platas-Iglesias, H. van Bekkum and J. A. Peters, *Magn. Reson. Chem.*, 2001, **39**, 723–726.

